Ocean Engineering 164 (2018) 414–425

Contents lists available at ScienceDirect

Ocean Engineering

journal homepage: www.elsevier.com/locate/oceaneng

Estimation of hydrodynamic derivatives of a container ship using PMM simulation in OpenFOAM

Hafizul Islam, C. Guedes Soares*

Centre for Marine Technology and Ocean Engineering (CENTEC), Instituto Superior Técnico, Universidade de Lisboa, Portugal

ARTICLE INFO

Keywords:
Static drift
Pure sway
Pure yaw
PMM
Hydrodynamic derivatives
KCS
OpenFOAM

ABSTRACT

Static drift, pure sway and pure yaw simulation results are determined for a container ship. For simulation, open source RANS solver, OpenFOAM was used. The simulation results were compared with two sets of experimental data. Next, hydrodynamic derivatives were predicted from simulation results and compared with experimental ones. The results show good agreement with experimental data, except for some pure yaw cases. Overall, the paper concludes that OpenFOAM is well capable of estimating hydrodynamic derivatives maintaining reasonable accuracy and computational efficiency.

1. Introduction

Maneuverability prediction in the design stage is among the key requirements in ship design to ensure safety and reliability. Traditionally, ship maneuverability characteristics are determined using model tests, which are both expensive and time-consuming. However, with the development of different computational fluid dynamics (CFD) tools and improvement in computational power, designers and researchers are focusing more on CFD to predict ship's seakeeping and maneuverability characteristics.

Ship designers use a number of ways to predict ship maneuverability characteristics in design stage like, theoretical approach, utilization of full-scale database, application of empirical method (Kijima and Nakiri, 2003), model test (Sutulo and Guedes Soares, 2006) and numerical approach using CFD. Theoretical approaches are mostly limited to slender bodies and fail to consider hull and appendage interaction. Utilization of full-scale data is only possible when similar ship models are already in operation. Applications of empirical formulas are also limited to particular hull forms or availability of data. Model tests are among the most popular methods for maneuverability prediction. One common method used in the experimental study to determine ship maneuverability properties is the captive model test, which includes oblique towing test (OTT), rotating arm test (RAT), circular motion test (CMT) and planar motion mechanism (PMM). Similar tests can also be performed using CFD, depending on the capabilities and extent of the solver being used.

The incorporation of CFD in ship maneuverability prediction has been relatively recent. Most of the early works related to CFD based maneuvering were focused on planar motion mechanism (PMM) simulations. Among the early researchers to discuss ship maneuverability using CFD were Simonsen and Stern (2005), Cura-Hochbaum (2006) and Wilson et al. (2006). However, PMM simulations were first widely discussed in SIMMAN 2008 workshop (SIMMAN, 2008), where different research groups presented static drift, pure sway, and pure yaw simulation results. Broglia et al. (2008) showed pure sway and pure yaw motion results for KVLCC1 and 2 models with propeller and rudder simulated using a solver developed by INSEAN. Cura-Hochbaum et al. (2008) simulated static drift, pure sway and pure yaw case for the two tanker models with propeller and rudder, using a self-developed code. Gullmineau et al. (2008) provided PMM results for US Navy frigate using ISIS-CFD solver. Miller (2008) provided PMM calculation for DTMB 5415 using CFDShip-Iowa. Wang et al. (2011) simulated oblique motion for KVLCC2 in deep and shallow water using commercial code FLUENT. Simonsen et al. (2012) presented zig-zag, turning circle and PMM results for an appended KCS model using STAR-CCM+ and compared them with experimental data. Lee et al. (2015) performed PMM simulation for a wind turbine installation vessel using OpenFOAM, ignoring free surface calculation. Later, Shen et al. (2015) incorporated dynamic overset grid in OpenFOAM and presented zig-zag simulation results with self-propulsion. Kim et al. (2015) presented PMM simulation results for KCS model using in-house code SHIP_Motion and predicted hydrodynamic derivatives from simulation results. Hajivand and Mousavizadegan (2015a,b) also performed PMM simulation using STAR-CCM+ and OpenFOAM (static drift only) for DTMB

* Corresponding author.
E-mail address: c.guedes.soares@centec.tecnico.ulisboa.pt (C. Guedes Soares).

https://doi.org/10.1016/j.oceaneng.2018.06.063
Received 23 October 2017; Received in revised form 20 February 2018; Accepted 22 June 2018
Available online 05 July 2018
0029-8018/

5512 model and predicted hydrodynamic derivatives from the simulation results. Recently, Yao et al. (2016) presented static drift, turning and pure sway simulation data using OpenFOAM for tanker model KVLCC2.

Although maneuvering related simulations are gaining popularity lately, their applications are mostly limited to large research groups and designers, who have sufficient resources and access to well-developed in-house or commercial codes. An alternative and economic solution to commercial and in-house codes may be the use of the open source CFD toolkit, OpenFOAM. Several researchers have already demonstrated the capability of OpenFOAM in performing maneuverability based simulations for different ship models. However, they were either limited to static cases, or avoided free surface consideration. Furthermore, existing papers do not discuss about the required settings for running such simulations. This paper aims at contributing to the field by presenting static drift, pure sway and pure yaw simulation results for a container ship model (KCS) using OpenFOAM, and estimating the hydrodynamic derivatives for it. The paper aims at demonstrating OpenFOAM's capability in performing maneuvering simulations, with detail regarding the mesh dependency and related solver-setup. It also intends to show that the toolkit is able to perform maneuvering simulations with reasonable accuracy, good efficiency and economy.

2. Method

2.1. Simulation solver

2.1.1. Mathematical model

OpenFOAM (Open Field Operation and Manipulation) is an open source library, written in C++ language following object-oriented paradigm. The code is available under GNU General Public License (GPL). It can be used to numerically solve a wide range of problems in fluid dynamics, from laminar to turbulent flows, with single and multiphases. It can solve both structured and unstructured polyhedral meshes including h-refinement or hanging nodes and contains an extensive range of solvers to perform different types of CFD simulations. It has several packages to perform multiphase turbulent flow simulation for floating objects. OpenFOAM also allows relatively easy customization and modification of solvers, because of its modular design. The solver has been elaborately described by Jasak (1996, 2009).

The OpenFOAM solver used to perform ship hydrodynamic simulations for this paper simulates incompressible, two-phase flow. The governing equations for the solver are the Navier-Stokes equation (1) and continuity equation (2) for an incompressible laminar flow of a Newtonian fluid. In vector form, the Navier-Stokes and Continuity equation are given by

$$\rho\left(\frac{\partial v}{\partial t} + v.\ \nabla v\right) = -\nabla p + \mu\nabla^2 v + \rho g, \tag{1}$$

$$\nabla v = 0. \tag{2}$$

where v is the velocity, p is the pressure, μ is the dynamic viscosity, g is acceleration due to gravity, and ∇^2 is the Laplace operator. Further, the continuity equation is of the form

The Volume of Fluid (VOF) method is used to model fluid as one continuum of mixed properties. This VOF method determines the fraction of each fluid that exists in each cell, thus tracks the free surface elevation. The equation for the volume fraction is obtained as

$$\frac{\partial \alpha}{\partial t} + \nabla(\alpha U) = 0, \tag{3}$$

where U is the velocity field, α is the volume fraction of water in the cell and varies from 0 to 1, full of air to full of water, respectively.

The unstructured collocated Finite Volume Method (FVM) using Gauss theorem together with user-defined and implemented solution algorithm and time-integration schemes (Drikakis et al., 2007) is used to discretize the governing equations. Time integration is performed by a semi-implicit second-order, two-point, backward-differencing scheme. Pressure-velocity coupling is obtained through PIMPLE algorithm (Ferziger and Peric, 2008), a combination of SIMPLE and PISO. OpenFOAM incorporates three different turbulence models, k-ε, k-ω and SST k-ω. Turbulence is discretized using a 2nd order upwind difference. Turbulence for the presented simulations was modeled with the Reynolds-averaged stress (RAS) SST *k-ω* two-equation model. The parameters were calculated using common guidelines from an earlier study (Labanti et al., 2016).

2.1.2. Coordinate system

OpenFOAM follows a Cartesian coordinate system, if not specified otherwise. All systems are based on an origin point and coordinate rotation. The solver has a local and a global coordinate system. The local coordinate system is used to define the simulation domain, comparing to global reference point. The global and local coordinate system might be same or different depending on the simulation. In ship simulation, where there is flowing fluid, the local and global coordinates, both are defined using Cartesian coordinate system. The local coordinate systems are generally right handed. The x-axis is positive from stern to bow direction, y is positive at star board side and z is positive upwards, as shown in Fig. 1.

2.1.3. Boundary conditions

The control volume represented a deep water condition, so the two lateral sides and the bottom were symmetry plane type faces; no additional information was required for this kind of boundary condition. Inlet, outlet, and atmosphere were patch faces with specific boundary condition for each one, and hull had a wall type boundary. For the presented simulation cases, boundary conditions used for the fluid properties and turbulence parameters are as shown in Table 1.

Here, FV is fixedValue (Dirichlet Boundary Condition), specified by the user, OPMV is outlet Phase Mean Velocity, PIOV is pressure Inlet Outlet Velocity that applies zero-gradient for outflow, whilst inflow velocity is the patch-face normal component of the internal-cell value and MWV is moving Wall Velocity. FFP is fixed Flux Pressure that adjusts the pressure gradient such that the flux on the boundary is that one specified by the velocity boundary condition; ZG is zero Gradient (Neumann Boundary Condition); TP is total Pressure, calculated as static pressure reference plus the dynamic component due to velocity. IO is inlet Outlet that provides a zero-gradient outflow condition for a fixed value inflow. kqRWF is the wall function for the turbulence kinetic energy, nutkRWF is rough wall function for kinetic eddy viscosity and omegaWF is the wall function for frequency.

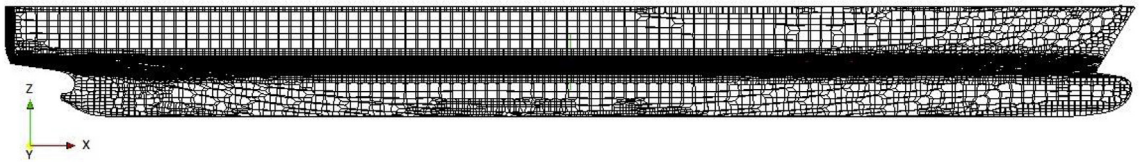

Fig. 1. Local Coordinate system in OpenFOAM.

Table 1
Boundary conditions used for the fluid properties and turbulence parameters in simulation.

	Inlet	Outlet	Atmosphere	Hull
U	FV	OPMV	PIOV	MWV
p_rgh	FFP	ZG	TP	FFP
α.water	FV	VHFR	IO	ZG
k	FV	IO	IO	kqRWF
nut	FV	ZG	ZG	nutkRWF
omega	FV	IO	IO	omegaWF

2.2. Ship model

The model ship used for this research is the KRISO Container ship (KCS). It is a 3600TEU capacity container ship designed by KRISO (formerly MOERI) for research purpose. The ship model is very popular among researchers, as many of its experimental and CFD data are openly available and has been discussed in Gothenburg, Tokyo, and SIMMAN workshops. Fig. 2 shows the hull shape and body plan of KCS model (SIMMAN, 2008).

For validation of CFD results, two different experimental fluid dynamics (EFD) data were used in this paper. The experiments were performed by Hyundai Heavy Industries (HHI) and Changwon National University (CWNU) (Kim et al., 2015). The basic dimensions of the model ships are shown in Table 2, along with the actual ship dimensions. The CFD simulations were performed in HHI model scale.

2.3. Simulation mesh

The domain size (blockMesh) for simulations was set following general ITTC (2011) guidelines; the inlet was placed two ship length windward the bow, the outlet four ship length downstream the stern, each lateral boundary was two ship lengths away from the ship's symmetry plane, the depth or bottom of domain was set at one ship length and the atmosphere was at half ship length from free surface.

The hull form was integrated to the blockMesh by using snappyHexMesh utility, which created a “body fitted” hexahedral mesh around the hull surface from the specified STL file. The drift angles for simulations were applied to STL files and then snappyHexMesh was executed. As for sway simulation, sway motion was obtained by using dynamic mesh directory. In blockMesh, the region near the hull form was refined four times using topoSet and snappyHexMesh was configured to perform single refinement near free surface and hull.

For investigating the grid dependency of the solver, three mesh resolutions were used maintaining a refinement ratio of roughly √2. All simulations were performed with full hull (both starboard and port side). The mesh resolutions used were of 1.68 million (fine), 1.1 million (mid) and 0.4 million (coarse), for Froude number 0.26. The simulations were performed using LTSInterFoam solver. The grid based uncertainty analysis performed for KCS model in OpenFOAM is shown in the equations, s = ± 1, depending on the sign of the convergence. Rest of the parameters are defined in Table 3.

Table 3. The analysis shows that the meshes show good convergence for the drift cases, except at 0-degree cases. After analysis, the medium mesh density (1.1 million) was chosen for simulations.

The grid dependency analysis was performed by following the procedure prescribed by Celik et al. (2008). The method is mainly based on Richardson extrapolation and is well accepted in scientific

Table 2
Principal dimensions of KCS (actual and model ship).

	Full scale ship	HHI Model	CWNU Model
Scale	1	40	322
Lpp (m)	230	5.75	0.7143
T (m)	10.8	0.27	0.0335
Bwl (m)	32.2	0.805	0.1
Displacement (m^3)	52030	0.813	0.001558
CB	0.651	0.651	0.651
CM	0.985	0.985	0.985
LCG (m)	−3.4	−0.058	−0.01056
Ship speed (m/s)	12.35	1.952	0.69
Froude number	0.26	0.26	0.26
Reynolds number	2.1×10^9	8.4×10^6	3.7×10^5

community. Conventionally, the mesh resolution used for the study is slightly coarse. However, in case of PMM simulation, only lateral pressure force and yaw moment are considered and forward frictional force is ignored, which allows application of relatively lower mesh resolution near the hull surface. The longitudinal and lateral force, and the yaw moment results were considered to check mesh sensitivity.

For the analysis, the grid refinement is performed in all x, y and z axis, maintaining same refinement ratio. The order of accuracy, p and Grid Convergence Index (GCI) are predicted using the following equations,

$$p = \frac{1}{\ln(r_{21})} \left| \ln \left| \varepsilon_{32} / \varepsilon_{21} \right| + \ln\left(r_{21}^{p} - s / r_{32}^{p} - s \right) \right| \quad (4)$$

$$\mathrm{GCI}_{\mathrm{fine}}^{21} = 1.25 e_a^{21} / (r_{21}^{p} - 1) \quad (5)$$

In the equations, s = ± 1, depending on the sign of the convergence. Rest of the parameters are defined in Table 3.

As can be seen from the analysis, the results show both monotonous and oscillatory convergence. This may be contributed to the very low mesh resolution used for the coarse mesh cases. Moreover, the target for the simulations was to properly capture the lateral force and yaw moment. Thus, meshing was done focusing on capturing lateral forces and moments, not longitudinal forces. As a result, poor convergence and high uncertainty are observed in longitudinal force (Fx) prediction. However, the uncertainty (GCI) is much lower for lateral force and yaw moment. Overall, the applied resolution is sufficient to attain reliable results with low uncertainty.

Fig. 3 shows general mesh configuration for the total domain, free surface and hull form. For capturing the sway and yaw amplitude region properly, refinement area used in sway simulation mesh was larger, comparing to drift simulation. Thus, the mesh used for sway and yaw simulations had higher resolution (1.6 million cells) comparing to drift simulation mesh. Furthermore, in order to accommodate the sway motion, interDyMFoam solver was used for sway simulation, instead of LTSInterFoam.

2.4. Computational resources

The simulations were performed in a single node Intel(R) Core i5 CPU with 4 cores, clock speed 2.27 GHz and 8 GB of physical memory. The average time step used was 0.001 s and for simulating each case with stable output, the required physical time was about 18 h per case. All the simulations were run up to 35 s (simulation time) for attaining stable results.

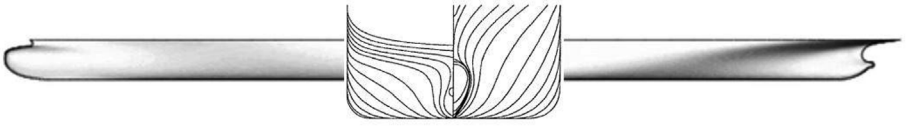

Fig. 2. Hull shape and body plan of KCS model.

Table 3
Uncertainty analysis of KCS model for static drift simulation in OpenFOAM.

Drift angle		Drag Force, F'x (x e3)			Lateral Force, F'y (x e3)			Yaw moment, M'z (x e3)		
		0.0	6.0	12.0	0.0	6.0	12.0	0.0	6.0	12.0
Output values	$Ø_1$ (fine)	−1.383	−1.963	−3.547	0.005	0.565	1.490	0.001	0.350	0.740
	$Ø_2$ (mid)	−1.302	−1.802	−3.663	0.013	0.552	1.615	0.005	0.346	0.720
	$Ø_3$ (cors)	−1.253	−1.954	−4.000	0.026	0.625	1.700	−0.01	0.320	0.716
Refinement ratio	$r_{21} = h_2/h_1$	1.50	1.50	1.50	1.50	1.50	1.50	1.50	1.50	1.50
	$r_{32} = h_3/h_2$	1.42	1.42	1.42	1.42	1.42	1.42	1.42	1.42	1.42
Convergence	$\varepsilon_{21/\varepsilon 32}$	1.67	−1.06	0.34	0.60	−0.17	1.47	−0.25	0.17	5.76
Order of accuracy	P	0.85	0.13	3.29	1.75	4.95	0.55	3.84	5.19	3.66
Grid convergence index (GCI)	GCI^{21}_{fine}	−0.178	−1.832	0.015	2.064	−0.004	0.419	0.863	−0.002	−0.010
	GCI^{32}_{fine}	−0.135	2.187	0.053	1.541	0.035	0.310	−1.29	−0.018	−0.002

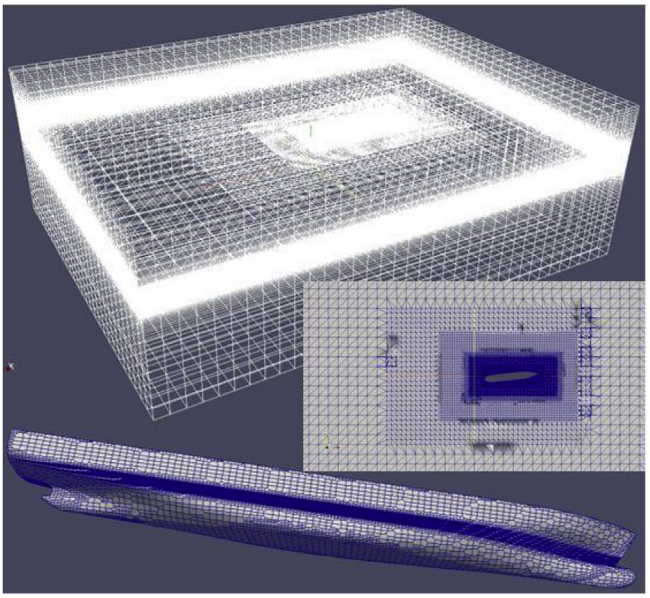

Fig. 3. Simulation mesh; overall simulation domain, mesh distribution on the free surface (drifted hull) and mesh distribution on hull form.

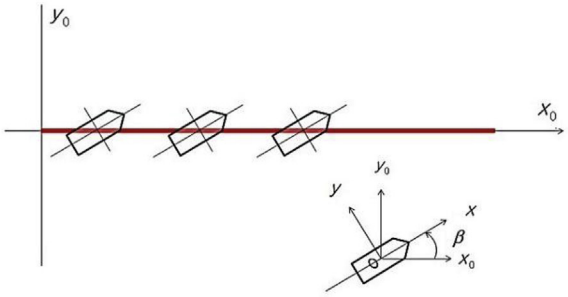

Fig. 4. Schematic diagram representing static drift motion.

Table 5
Static drift simulation results for KCS model using LTSInterFoam.

Drift Angle Degrees	Lateral Force', F'y (xe-3) CFD	Lateral Force', F'y (xe-3) EFD (HHI)	Lateral Force', F'y (xe-3) EFD (CWNU)	Yaw Moment', M'z (xe-3) CFD	Yaw Moment', M'z (xe-3) EFD (HHI)	Yaw Moment', M'z (xe-3) EFD (CWNU)
0	−0.01	0.005	0.008	0.005	−0.03	0.012
2	0.22	–	0.07	0.098	–	0.11
4	0.37	–	0.29	0.221	–	0.24
6	0.55	0.61	0.53	0.346	0.34	0.34
8	0.80	–	0.83	0.476	–	0.43
10	1.15	–	1.13	0.591	–	0.52
12	1.61	1.64	1.50	0.720	0.75	0.62

3. Results

The static drift simulations were performed with static mesh and LTSInterFoam solver was used, whereas, for pure sway and yaw simulation, dynamic mesh with interDyMFoam solver was used. Drift simulations were performed for six different drift angles, sway simulations for seven sway rates, and yaw simulations for six yaw rates. From each simulation result, lateral force and yaw moment were calculated. Later, hydrodynamic derivatives were calculated from their slopes.

3.1. Static drift simulation

Static drift test is the towing of the ship in a tank in oblique condition, as shown in Fig. 4, where β represents the drift angle. For simulations, the same conditions were reproduced in CFD environment using OpenFOAM. All simulations were performed at the static condition, that is, all ship motions were restricted. Initially, simulations were run using LTSInterFoam and interFoam for two drift cases. LTSInterFoam presented better results comparing to interFoam as shown in Table 4. Thus, LTSInterFoam was preferred to perform rest of the simulations. As for interDyMFoam, the solver took a longer time to produce stable results for static simulations, which required longer resource allocation, thus it was avoided.

For validation of results, two sets of experimental data were used, which were reported by Kim et al. (2015). The experiments were

Table 4
Comparison of simulation results between LTSInterFoam and interFoam.

Drift Angle (Degs.)	Lateral Force', F'y (xe-3) CFD		Lateral Force', F'y (xe-3) EFD (HHI)	Lateral Force', F'y (xe-3) EFD (CWNU)	Yaw Moment', M'z (xe-3) CFD		Yaw Moment', M'z (xe-3) EFD (HHI)	Yaw Moment', M'z (xe-3) EFD (CWNU)
	LTSInterFoam	interFoam			LTSInterFoam	interFoam		
6	0.55	0.56	0.61	0.53	0.346	0.347	0.34	0.34
12	1.61	1.69	1.64	1.50	0.720	0.719	0.75	0.62

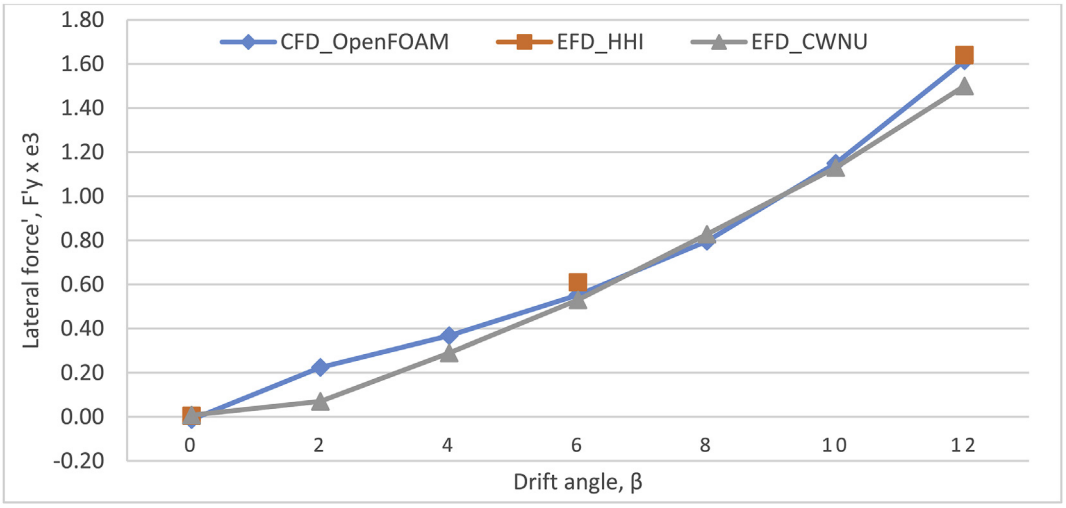

Fig. 5. Non-dimensional lateral force experienced by KCS model at different drift angles.

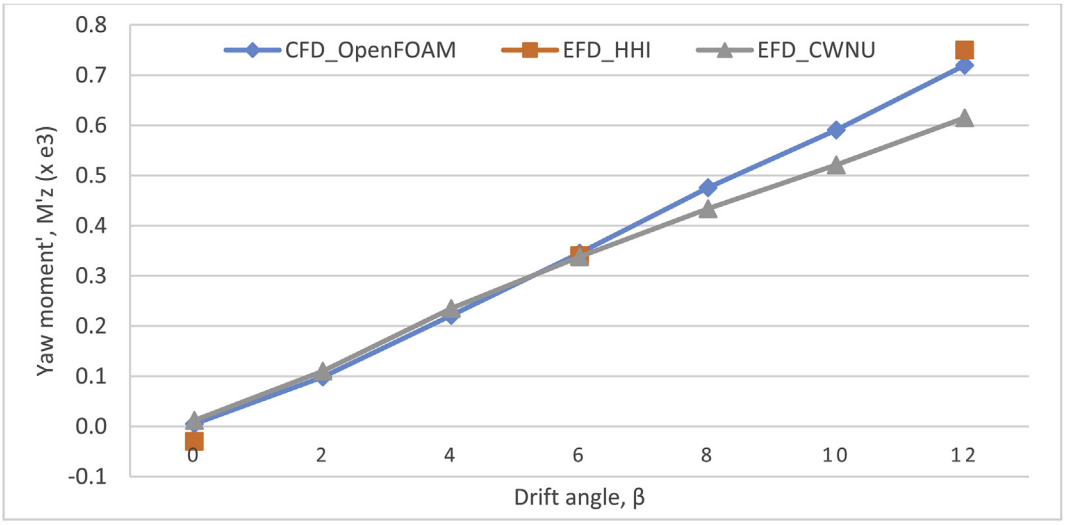

Fig. 6. Non-dimensional yaw moment experienced by KCS model at different drift angles.

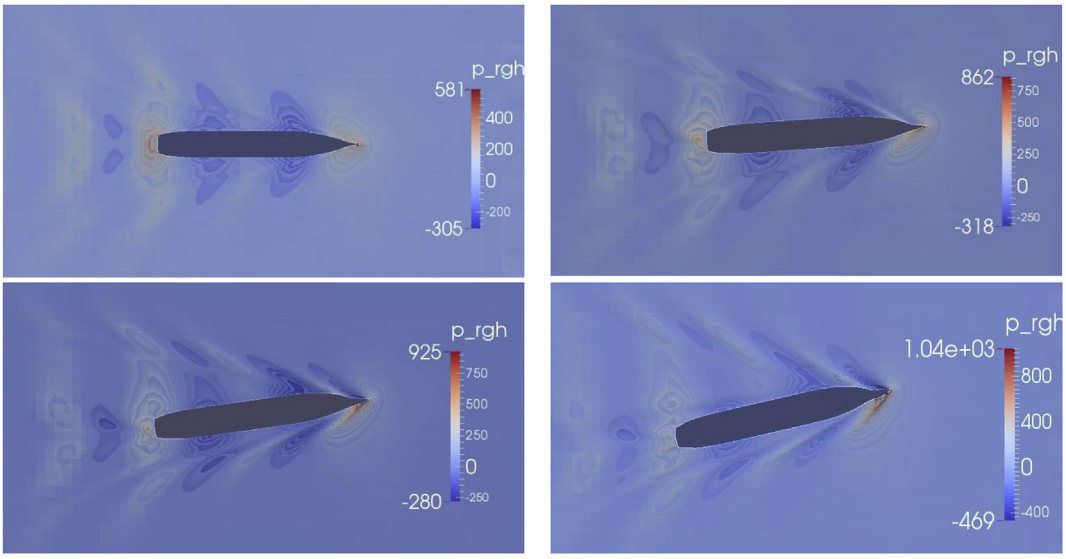

Fig. 7. Hydrodynamic pressure distribution on the free surface during drift motion of KCS; 0° (top left), 4° (top right), 8° (bottom left) and 12° (bottom right).

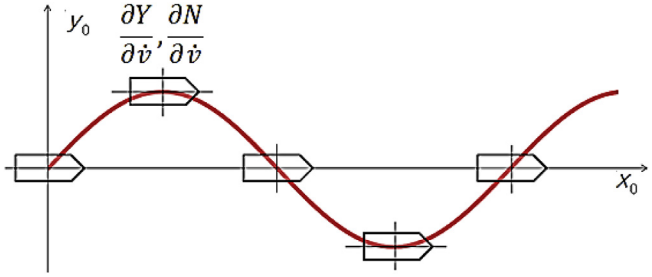

Fig. 8. Schematic diagram representing pure sway motion.

Table 6
Pure sway simulation results for KCS model using InterDyMFoam.

Sway rates, v'_{max}	Lateral Force', F'y (xe-3) CFD_OpenFOAM	Lateral Force', F'y (xe-3) EFD (HHI)	Lateral Force', F'y (xe-3) EFD (CWNU)	Yaw Moment', M'z (xe-3) CFD_OpenFOAM
−0.02	0.06	–	−0.003	0.05
−0.05	0.17	–	–	0.12
−0.08	0.31	–	–	0.18
−0.084	–	–	0.32	–
−1.0	0.40	0.36	–	0.22
−1.5	0.67	–	–	0.33
−1.9	–	–	0.85	–
−2.0	0.95	0.87	–	0.43
−2.5	1.29	–	–	0.55
−3.0	1.63	1.18	–	0.68
−3.4	–	–	1.52	–

performed by Hyundai Heavy Industry (HHI) and Changwon National University (CWNU). HHI performed three runs with 0, 6 and 12-degree drift, and CWNU performed eight runs with drift angle varying from 0 to 14°, with a 2-degree interval. Simulations were run from 0 to 12° using 2-degree interval. All the simulations were performed in HHI model scale. For lateral force and yaw moment non-dimensionalization, following equations were used, as reported by Kim et al. (2015).

$$F'_Y = \frac{f_y\,(N)}{\rho \times v^2 \times L_{pp}^2} \tag{6}$$

$$M'_Z = \frac{m_z\,(N-m)}{\rho \times v^2 \times L_{pp}^3} \tag{7}$$

The static drift simulation results are shown in Table 5, which is graphically represented in Fig. 5 and Fig. 6.

As can be seen from the results, the simulation results well capture the trend of lateral force and yaw moment. The two sets of experimental data show slight disagreement with each other. Considering the scale of test models and test facilities, such difference is natural. For the simulations, since HHI model was used, results show better agreement with HHI data. The results indicate that with increasing drifting angle, the lateral force and yaw moment encountered by the ship increases. Thus, with increasing drift angle, higher power is required for propulsion.

Fig. 7 shows pressure distribution on free surface at drift angles 0, 4, 8 and 12°, respectively. As can be seen, in drift motions, maximum resistance is encountered by the ship bow front. With the increase in drift angle, pressure encountered by the ship also increases, so does free surface deformation.

3.2. Pure sway simulation

In pure sway test, sway motion is applied on ship hull form externally, and all ship motions are restricted. A schematic diagram of sway motion is shown in Fig. 8. To reproduce sway motion test in CFD medium, sway motion was applied externally on the simulation domain and all ship motions were kept restricted. The simulations were performed with a dynamic mesh using interDyMFoam solver of OpenFOAM, where sway motion was applied by selecting oscillatingLinearMotion module of solidBodyMotionFunction in the dynamicMeshDict. The sway motion applied on the domain is defined by the following equation.

$$y_o = \eta_{\text{sway}} \sin(\omega t) \tag{8}$$

η_{sway} is sway amplitude and ω is frequency, which is $\frac{2\pi}{T}$. T is the period of one cycle. The maximum y-axis acceleration is $\omega^2\eta_{sway}$.

In simulations, the frequencies were kept constant and sway amplitudes were adjusted for different sway rates. Simulations were performed for eight different sway rates and were compared with experimental cases presented by HHI and CWNU. HHI presented results for three different sway rates, whereas, CWNU presented four. The sway forces were measured at maximum sway displacement, where sway

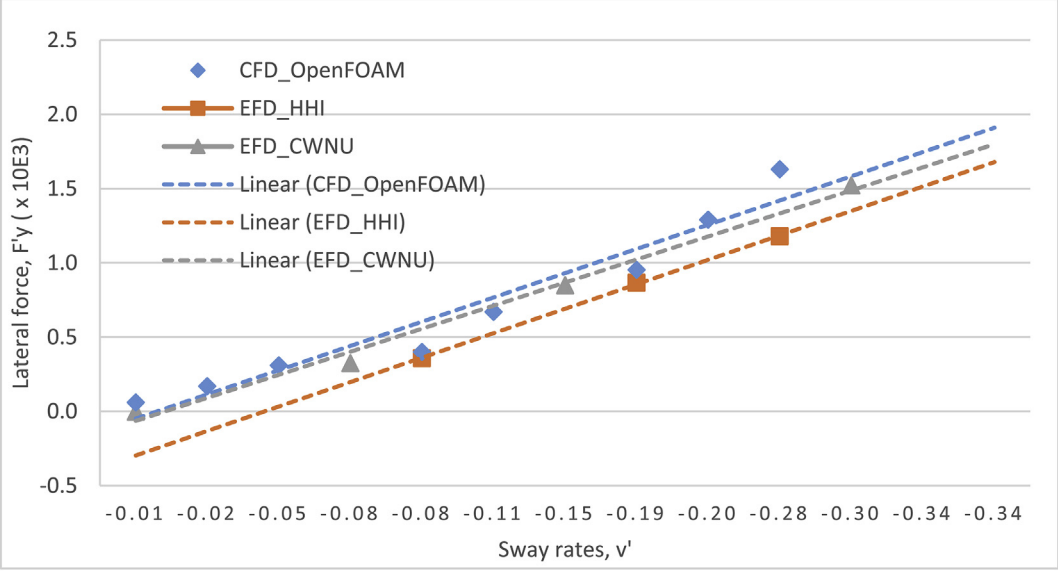

Fig. 9. Non-dimensional lateral force experienced by KCS model at different sway rates.

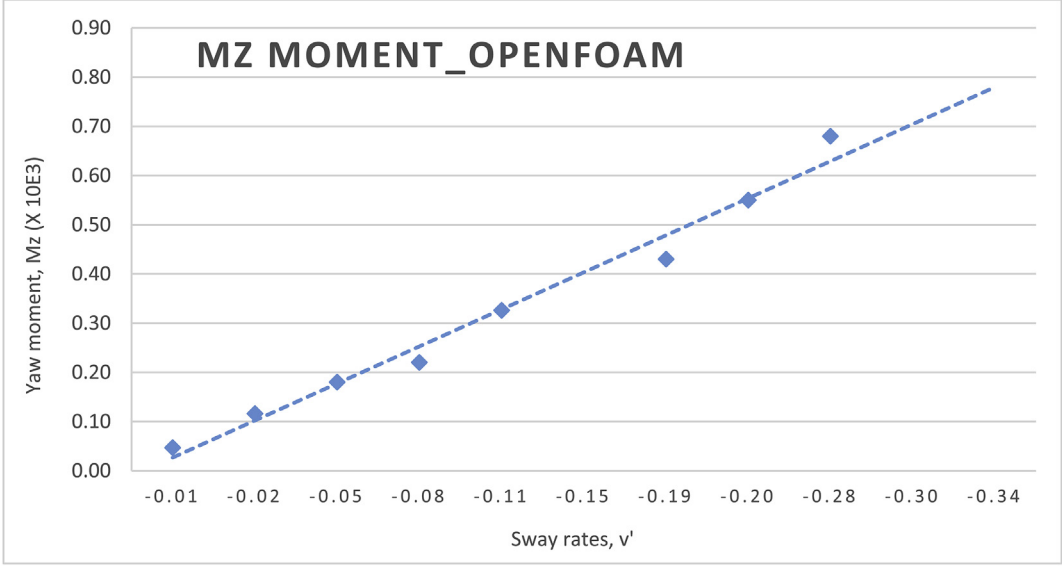

Fig. 10. Non-dimensional yaw moment experienced by KCS model at different sway rates.

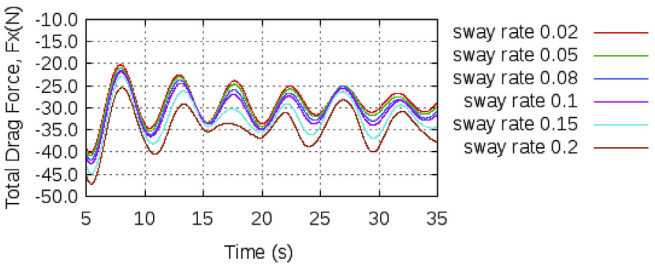

Fig. 11. Time history for drag force in sway simulation.

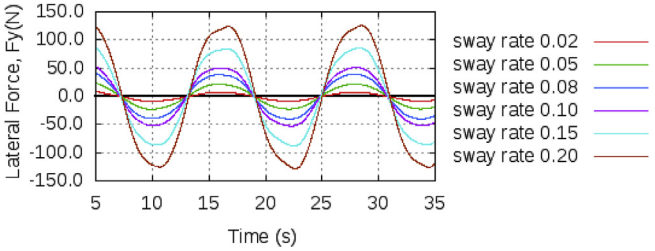

Fig. 12. Time history for lateral force in sway simulation.

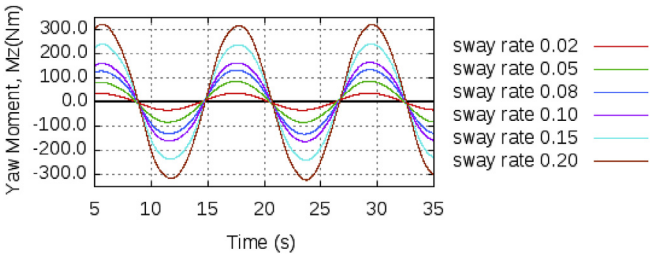

Fig. 13. Time history for yaw moment in sway simulation.

velocity is maximum and acceleration is minimum. For non-dimensionalization of sway forces and z moments, the same equations (6) and (7) mentioned in static drift cases were used.

The pure sway simulation results are shown in Table 6. All simulations were performed at Froude number 0.26. Although simulations were performed for a large number of sway rates, the number of available experimental data for sway cases are limited. Furthermore, Kim et al. (2015) only presented experimental data for sway forces, in his paper, not for z moments. Thus, comparison of moment results was not possible. The comparison of lateral force prediction between CFD and EFD are shown in Fig. 9. The linear trend lines were generated using regression for all three data set. The figure shows that, although there are deviations among CFD and EFD data, CFD results well follow the trend line of HHI EFD data. Fig. 10 shows the maximum yaw moment prediction at different sway rates.

Time history for simulation results showing longitudinal force, lateral force and yaw moment at different sway rates are shown in Fig. 11, Fig. 12 and Fig. 13. The time histories show the gradual increase in forces and moment encountered by the ship with increasing sway rate.

The sway motion creates a rapid change of pressure in the lateral direction. Depending on the ship's position on sway path, pressure distribution on the free surface and on the hull for port and starboard side are found to be different.

Fig. 13 shows pressure distribution on the zero surface for a KCS model in pure sway motion at sway rate 0.2. The ship's positions at the sway path are shown in the bottom right figure. Pressure distribution on the hull surface is shown in Fig. 15 for the same positions.

3.3. Pure sway simulation

Similar to previous case, in pure yaw, yaw motion is applied externally on ship hull form, keeping other ship motions restricted. A schematic diagram of yaw motion is shown in Fig. 16. To reproduce yaw motion test in CFD medium, yaw motion was applied externally on the simulation domain and all ship motions were kept restricted. The simulations were performed with a dynamic mesh using interDyMFoam solver of OpenFOAM, where yaw motion was applied by coupling oscillatingLinearMotion and oscillatingRotatingMotion, using multiMotion module of solidBodyMotionFunction in the dynamicMeshDict. A cosine function was used in the oscillatingRotatingMotion module to impose the yaw angle and a sine function in the oscillatingLinearMotion to update the ship position following the yaw angle. An initial acceleration period was also imposed to ensure gradual positioning of the ship to maximum yaw angle (see Fig. 17).

The yaw motion applied on the domain is defined by the following equation.

$$\psi = -\psi_0 \cos(2\pi\omega t) \tag{9}$$

$$r_{PMM} = \psi_0(2\pi\omega)\sin(2\pi\omega t) \tag{10}$$

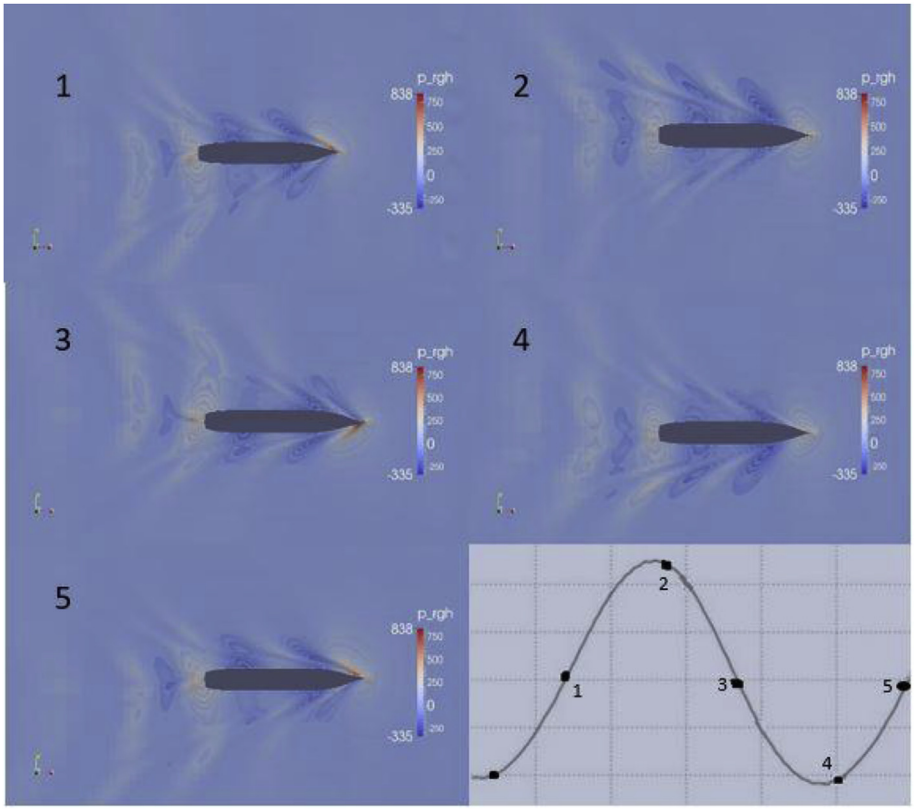

Fig. 14. Hydrodynamic pressure distribution on zero surface during pure sway motion at sway rate 0.2 (figure at bottom right shows ship positions at sway path).

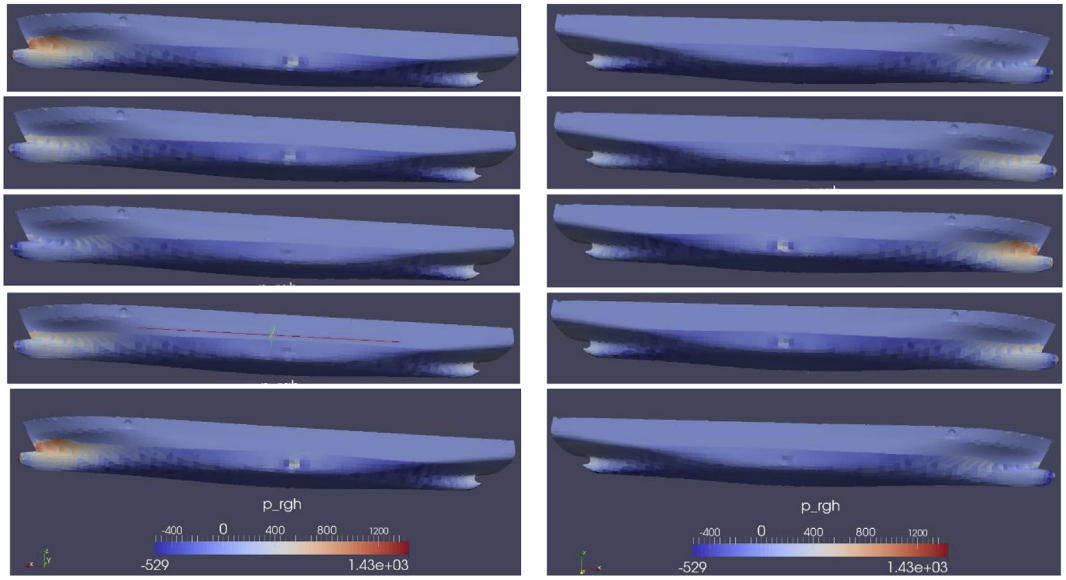

Fig. 15. Hydrodynamic pressure distribution (model scale) on hull surface (in left, portside; in right, starboard side) during pure sway motion at sway rate 0.2. Ship's positions (from top to bottom) in sway path are same as shown in Fig. 14.

$$\dot{r}_{PMM} = \psi_0(2\pi\omega)^2 \sin(2\pi\omega t) \tag{11}$$

$$r' = max(r_{PMM}) * L_{PP}/U \tag{12}$$

ψ_0 is the yaw amplitude [rad], ψ is the heading angle and ω is the frequency, which is $\frac{2\pi}{T}$. T is the period of one cycle. r_{PMM} is the yaw rate and $\dot{r}_{PMM}$ the yaw acceleration. And r' is the non-dimensionalized yaw velocity.

All the simulations were performed at the design Froude number of 0.26, and mesh resolution was kept the same as the pure sway case (1.6 million). In the simulations, the yaw angle was kept constant and the frequency and sway position was adjusted according to the yaw rate. Total seven cases were simulated with varying yaw rate. The case settings are shown in Table 7.

The simulation results were compared with experimental data provided by HHI and CWNU (Kim et al., 2015). However, the data from HHI was limited to three cases and for CWNU it was six. Furthermore, due to different yaw angle settings, the yaw acceleration rate observed in the experimental and CFD cases are different. In case of pure yaw

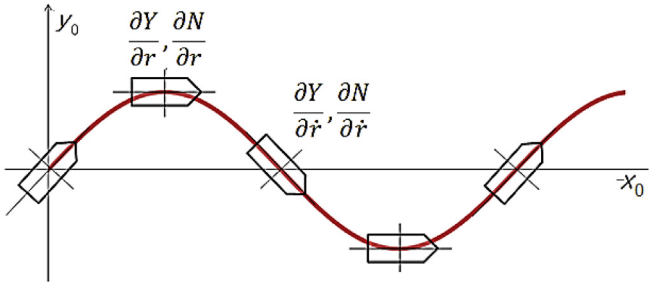

Fig. 16. Schematic diagram representing pure yaw motion.

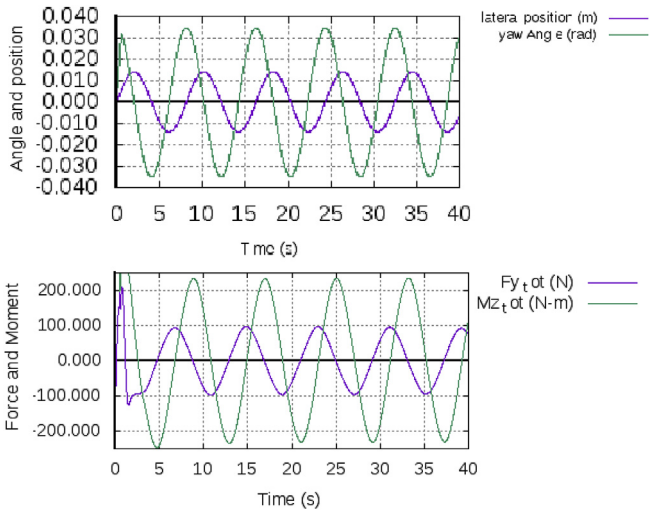

Fig. 17. Time history for the yaw angle and sway position, and lateral force and yaw moment at yaw rate 0.50.

Table 7
Simulation parameter settings for pure yaw simulation.

No	r'	Max yaw angle (deg)	Frequency (Hz)	Max lateral displacement (m)	rdot'
1	0.1	2	0.1548	0.0701	0.2865
2	0.15	2	0.2322	0.0467	0.6446
3	0.20	2	0.3096	0.0350	1.1459
4	0.30	2	0.4644	0.0234	2.5783
5	0.40	2	0.6191	0.0175	4.5837
6	0.50	2	0.7739	0.0140	7.1620

Table 8
Simulation and experimental results for lateral force and yaw moment for a KCS model with varying yaw rate. (x e−3).

r'	OpenFOAM		HHI		CWNU	
	Fx'	Mz'	Fx'	Mz'	Fx'	Mz'
0.1	−0.012	−0.004	–	–	–	–
0.15	−0.048	−0.010	–	–	−0.010	−0.140
0.20	−0.095	−0.026	–	–	−0.134	−0.207
0.25	–	–	–	–	–	–
0.30	−0.320	−0.094	−0.096	−0.340	−0.041	−0.332
0.35	–	–	–	–	–	–
0.40	−0.540	−0.140	−0.088	−0.442	−0.196	−0.431
0.50	−0.658	−0.160	−0.188	−0.541	–	−0.762
0.70	–	–	–	–	−0.808	−0.879

motion, there is a phase gap between the yaw angle and the lateral motion. When the yaw angle is maximum, lateral position or sway is at zero. And, when yaw is at zero, sway is at maximum. Fig. 13 shows the

Table 9
Simulation and experimental results for lateral force and yaw moment for a KCS model with varying yaw acceleration rate. (x e−3).

rdot'	OpenFOAM		HHI		CWNU	
	Fxr_dot'	Mzr_dot'	Fxr_dot'	Mzr_dot'	Fxr_dot'	Mzr_dot'
−0.15	–	–	–	–	−0.059	0.025
−0.28	0.270	0.208	–	–	−0.017	0.056
−0.38	–	–	0.118	0.106	–	–
−0.62	0.280	0.224	0.177	0.148	0.051	0.150
−0.85	–	–	0.287	0.218	–	–
−1.15	0.290	0.250	–	–	0.169	0.333
−1.77	–	–	–	–	0.481	0.590
−2.50	0.370	0.267	–	–	–	–
−3.48	–	–	–	–	1.494	0.738
−4.58	0.600	0.286	–	–	–	–

time history of the results for the simulation ran at 0.50 yaw rate. The figure shows that the peak value for lateral force is observed roughly when the yaw is at maximum, and the peak value for yaw moment is observed when yaw angle is minimum. Since different frequencies were used for each yaw simulation case, a combined time history for all the cases could not be presented here.

To determine the yaw derivatives, Yr and Nr, F'y and M'z should be estimated at minimum yaw angle amplitude, and for $Y_{\dot{r}}$ and $N_{\dot{r}}$, F'y and M'z should be estimated at maximum yaw angle amplitude (Lewis, 1988). Thus, for varying yaw rate, lateral force and yaw moment data were collected at zero yaw angle, and for varying yaw acceleration rate, lateral force and yaw moment were calculated at maximum yaw angle. The CFD simulation results, along with comparison with experimental data and simulation data are shown in Table 8 and Table 9. For better comparison, the results for varying yaw rate are also shown in Fig. 18 and Fig. 19, and for yaw acceleration rate in Fig. 20 and Fig. 21.

As can be seen from the results, the simulation results for varying yaw rate do not agree well with experimental data, however, the results well follow the trend line. Since the purpose of the simulations is to calculate the hydrodynamic derivatives, a well followed trend line is more important, comparing to accurate value prediction. Thus, for these cases a comparatively lower mesh resolution could be applied, which saved in computational expenses. Furthermore, even for the experimental data, the two results from HHI and CWNU do not agree very well with each other either. HHI provided only three results, which is insufficient to properly realize the result trend line.

In case of results for varying yaw acceleration rate, simulation results agree poorly with experimental data. Even the trend line could not be captured properly. This might be because of the low yaw angle applied for the simulations, comparing to the experimental cases. Furthermore, during pure yaw simulation, a sharp change in fluid flow is encountered from ship's bow and stern direction, during changing yaw angle. As the lateral force and yaw moment encountered is the sum of force and moment all through the hull surface, the changing flow pattern results into unstable predictions (Simonsen and Stern, 2008). This sharp change is often difficult to capture and requires high mesh resolution, with low time step. To demonstrate the change of pressure at the free surface due to yaw motion, pressure distribution at zero water level is shown in Fig. 22, for varying yaw angles at yaw rate 0.50.

3.4. Hydrodynamic derivatives prediction

Hydrodynamic derivatives or coefficients represent the rate of change in force or moment, with the rate of change in velocity or acceleration. The value of hydrodynamic derivatives help to determine the stability and maneuverability characteristics of a vessel, thus they are determined in advance to ensure proper functioning of a marine vehicle. Hydrodynamic coefficients are also known as added mass and damping coefficients. The added mass coefficients are acceleration

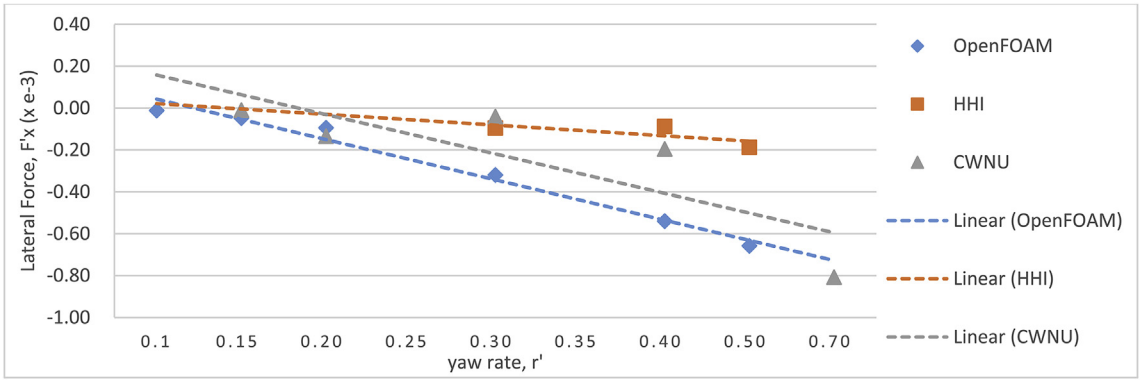

Fig. 18. Simulation and experimental results for lateral force for a KCS model with varying yaw rate.

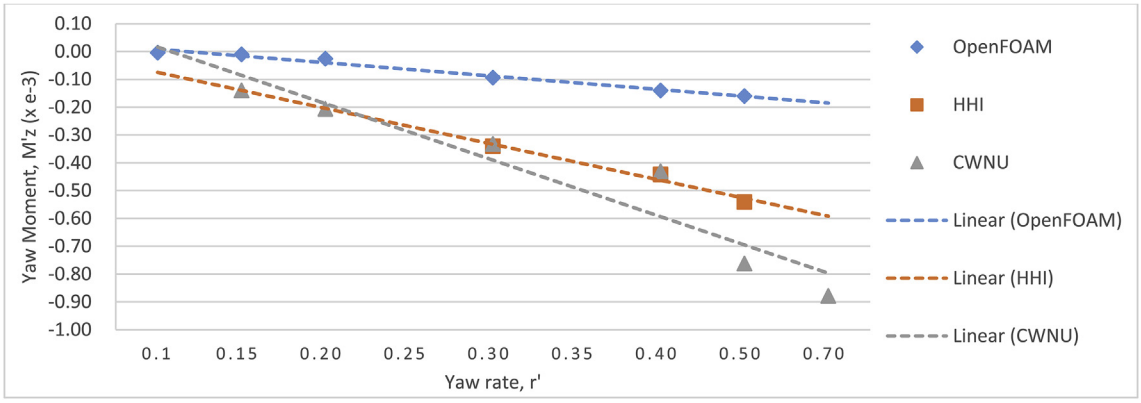

Fig. 19. Simulation and experimental results for yaw moment for a KCS model with varying yaw rate.

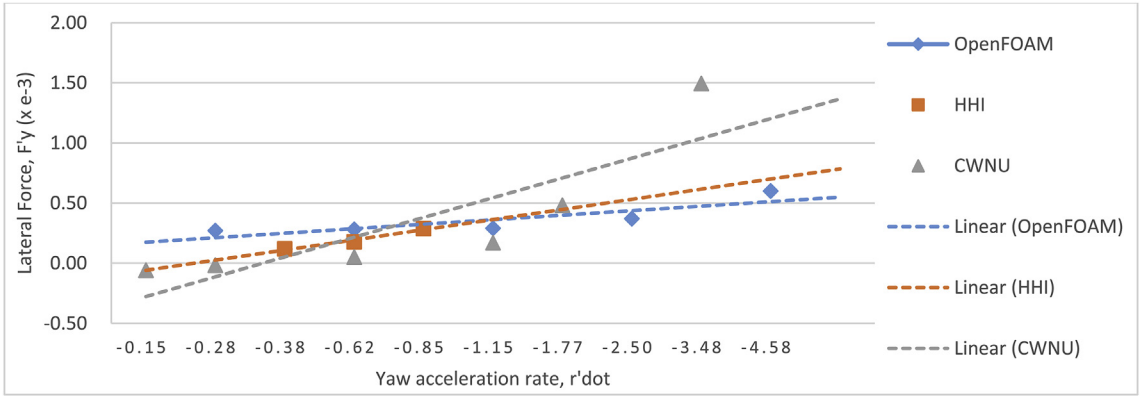

Fig. 20. Simulation and experimental results for lateral force for a KCS model with varying yaw acceleration rate.

dependent, whereas, the damping coefficients are velocity dependent. The added mass coefficients may be calculated through non-viscous fluid flow solution around the hull. The damping is caused by the wave formation in the free water surface and the viscosity effect. The total damping coefficient is predicted by solving viscous fluid flow around the vessel. Generally, captive model tests are used with conditions to derive these coefficients. Among captive tests, Planar Motion Mechanism (PMM) test is a very popular method used for deriving all the damping and added mass coefficients (Lewis, 1988).

In this paper, the hydrodynamic derivatives were predicted from lateral forces and yaw moments encountered by the ship model at different drift, sway and yaw conditions. By using curve fitting to the data for forces and moments as a function of drift angle β, sway rate *v'max, yaw rate r'max and yaw acceleration rate r'dot(max)*; the hydrodynamic derivatives or coefficients, X_{vv}, Y_v, Y_{vvv}, N_v, N_{vvv}, $Y_{\dot{v}}$, $N_{\dot{v}}$, Y_r, N_r, $Y_{\dot{r}}$ and $N_{\dot{r}}$ can be predicted. Among the derivatives, Y_v and N_v are linear, and rest are non-linear.

Although some of the non-linear derivatives can be predicted from static drift results, their reliability can be limited. Since experimental data is not available for comparison of all these non-linear derivatives, only linear derivatives were predicted from the drift results. Y_v was predicted from the slope of lateral motion F'y and N_v was predicted from the slope of yaw moment M'z. The slopes were generated using linear regression. The predicted results and comparison with EFD data are shown in Table 10. The results show reasonable agreement with CFD and EFD data.

Next, pure sway simulation results were used for predicting two non-linear derivatives. From pure sway simulations, derivatives $Y_{\dot{v}}$ and $N_{\dot{v}}$ were calculated. The derivatives were predicted from the slopes of peak sway forces (Fig. 9) and yaw moments (Fig. 10) at different sway

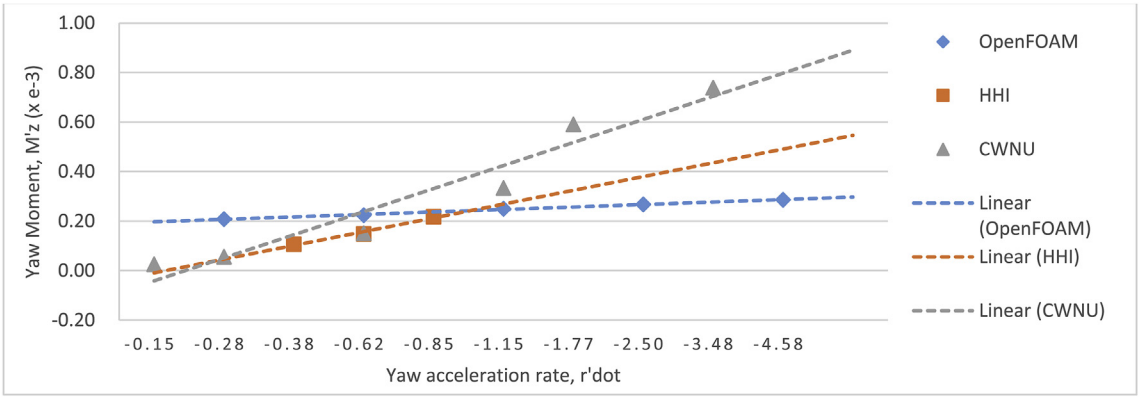

Fig. 21. Simulation and experimental results for yaw moment for a KCS model with varying yaw acceleration rate.

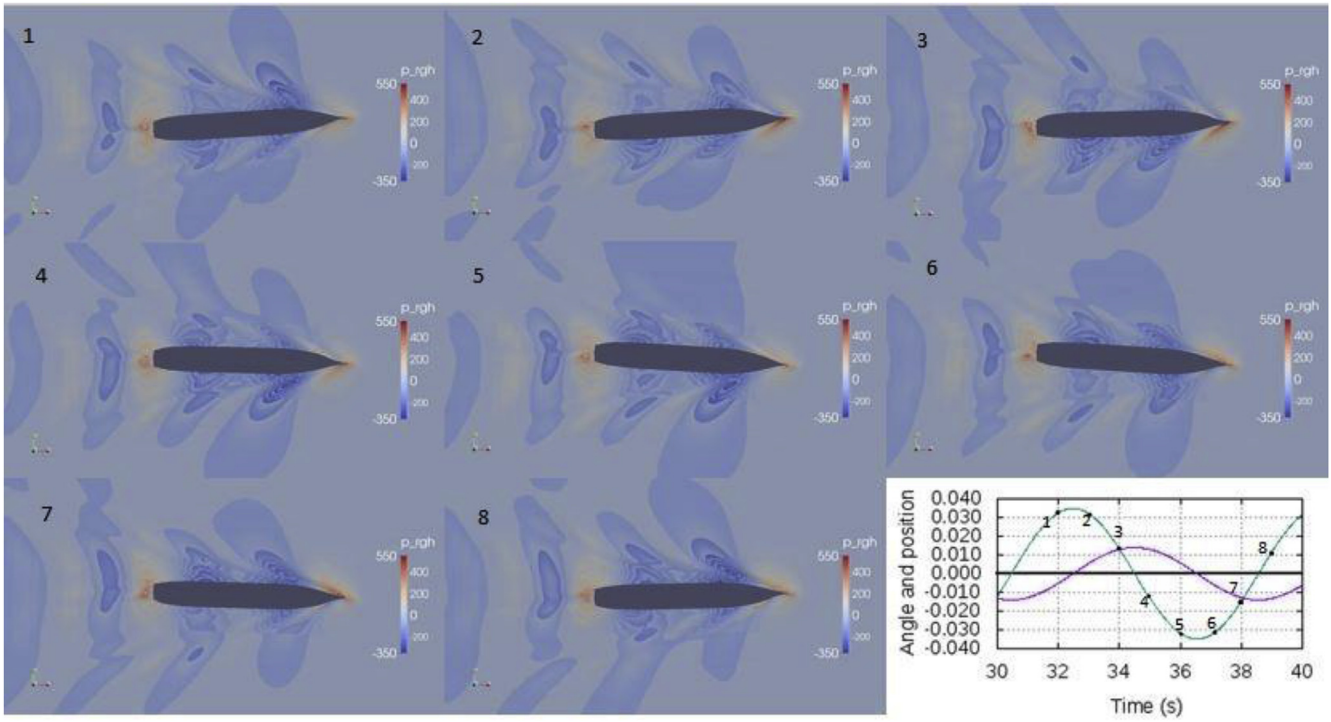

Fig. 22. Hydrodynamic pressure distribution on zero surface during pure yaw motion at yaw rate 0.5 (Figure at bottom right shows ship positions at yaw angle).

Table 10
Predicted linear hydrodynamic derivatives from static drift simulation results (x e−3).

Derivatives	CFD_OpenFOAM	EFD_HHI	Deviation%	EFD_CWNU	Deviation%
Y_v	0.136	0.136	0.5%	0.124	9.1%
N_v	0.060	0.065	7.7%	0.050	20%

Table 11
Predicted hydrodynamic derivatives from pure sway simulation results (x e−3).

Derivatives	CFD_OpenFOAM	EFD_HHI	Deviation%	EFD_CWNU	Deviation%
$Y_{\dot{v}}$	−4.1	−4.2	2.38%	−3.8	7.9%
$N_{\dot{v}}$	−2.1	–	–	–	–

rates. Linear regression was used to produce trend lines for CFD and EFD data, and from them, slopes were calculated. The hydrodynamic derivatives derived from pure sway simulation are shown in Table 11.

In both static drift and pure sway cases, hydrodynamic derivatives predicted by CFD show better agreement with HHI data, comparing to CWNU data. This may be because all the simulations were performed depicting HHI model test. Furthermore, considering the model scale used by CWNU, which was rather small, HHI results may be considered more reliable.

Finally, pure yaw simulation results were used to predict Y_r, N_r, $Y_{\dot{r}}$

Table 12
Predicted hydrodynamic derivatives from pure yaw simulation results (x e − 3).

Derivatives	CFD_OpenFOAM	EFD_HHI	Deviation%	EFD_CWNU	Deviation%
Y_r	−0.096	−0.026	270%	−0.094	2.13%
N_r	−0.024	−0.06	60%	−0.10	76%
$Y_{\dot{r}}$	0.037	0.084	56%	0.16	77%
$N_{\dot{r}}$	0.01	0.056	82%	0.093	89%

and $N_{\dot{r}}$ derivatives. Y_r and N_r were calculated from the lateral force and yaw moment for varying sway rate, and $Y_{\dot{r}}$ and $N_{\dot{r}}$ were calculated from varying yaw acceleration rate results. Linear regression was used to produce trend lines for CFD and EFD data, and from them, slopes were calculated. The hydrodynamic derivatives derived from pure yaw simulation are shown in Table 12.

As can be observed from the predicted yaw derivatives, the simulation results agree very poorly with experimental data. However, the experimental data themselves do not agree well with each other. Furthermore, for stability, $N_{\dot{r}}$ should have a negative value, which is not the case even for experimental data. For pure yaw case, HHI presented only three cases, which might be enough to get a proper representation of the force and moment trend line for yaw motion. Furthermore, for simulation, higher yaw angle may be needed to better predict the forces and moments, as mentioned in the previous section.

4. Conclusion

Prediction of ship hydrodynamic derivatives is an essential part of ship design to ensure that the design meets required stability and maneuverability characteristics. The paper presents the estimated value of some hydrodynamic derivatives of a container ship using CFD medium. The results show good agreement with experimental data, except for some of the pure yaw cases.

Simulations were performed for a KCS model at different static drift, pure sway and pure yaw conditions, and lateral forces and yaw moments were predicted. The predicted results show good agreement with experimental data. Later, hydrodynamic derivatives were calculated from the simulation results, which also are in reasonable agreement with experiments, except for yaw derivatives. The paper concludes that the open source CFD toolkit, OpenFOAM, is well capable of performing most of the maneuverability related simulations with reasonable accuracy, consuming minimum computational resources.

However, in the paper, it was only possible to predict drift and sway simulation results with reasonable accuracy using OpenFOAM. Further investigation is needed to improve the prediction results for pure yaw cases. The solver also shows higher deviation with experimental data at higher amplitude drift angles and sway rates. Thus, further research is needed to improve the predictions and incorporate other maneuverability related simulation capabilities to OpenFOAM.

Acknowledgments

The work was a part of SHOPERA (Energy Efficient Safe SHip OPERAtion) Collaborative Project which was co-funded by the Research DG of the European Commission (contract No. 605221) within the RTD activities of the FP7 Thematic Priority Transport/FP7-SST-2013-RTD-1/Activity 7.2.4 Improving Safety and Security/ SST.2013.4–1:Ships in operation http://shopera.org/.

References

Broglia, R., Muscari, R., Mascio, A.D., 2008. Numerical simulations of the pure sway and pure yaw motion of the KVLCC1 and 2 tankers. In: SIMMAN 2008 Proceedings, pp. F2–F9.
Celik, I.B., Ghia, U., Roache, P.J., Freitas, C.J., Coleman, H., Raad, P.E., 2008. Procedure for estimation and reporting of uncertainty due to discretization in CFD applications. J. Fluid Eng. Trans. ASME 130, 078001–078004.
Cura-Hochbaum, A., 2006. In: Virtual PMM Tests for Manoeuvring Prediciton. 26th Symposium on Naval Hydrodynamics, pp. 23-28, Rome, Italy.
Cura-Hochbaum, A., Vogt, M., Gatchell, S., 2008. Manoeuvring prediction for two tankers based on RANS simulations. In: SIMMAN 2008 Proceedings, pp. F22–F27.
Drikakis, D., Fureby, C., Grinstein, F., Liefendahl, M., 2007. ILES with limiting algorithms. In: In Implicit Large Eddy Simulation: Computing Turbulent Fluid Dynamics. s.l. Cambridge University Press, pp. 94–129.
Ferziger, J.H., Peric, M., 2008. Numerische Stromungsmechanik, second ed. Springer Verlag, Heidelberg, Berlin.
Gullmineau, E., Queutey, P., Visonneau, M., Leroyer, A., Deng, G., 2008. RANS simulation of a US Navy frigate with PMM motions. In: SIMMAN 2008 Proceedings, pp. F28–F33.
Hajivand, A., Mousavizadegan, S.H., 2015a. Virtual maneuvering test in CFD media in presence of free surface. Int. J. Nav. Architect. Ocean. Eng. 7, 540–558.
Hajivand, A., Mousavizadegan, S.H., 2015b. Virtual simulation of maneuvering captive tests for a surface vessel. Int. J. Nav. Architect. Ocean. Eng. 7, 848–872.
Jasak, H., 1996. Error Analysis and Estimation for the Finite Volume Method with Applications to Fluid Flows. Ph.D. thesis. Imperial College of Science, Technology & Medicine, London.
Jasak, H., 2009. OpenFOAM: open source CFD in research and industry. Int. J. Nav. Architect. Ocean. Eng. 1 (2), 89–94.
Kijima, K., Nakiri, Y., 2003. On the practical prediction method for ship manoeuvering characteristics. Transaction of the West Japan Society of Naval Architects 105, 21–31.
Kim, H., Akimoto, H., Islam, H., 2015. Estimation of the hydrodynamic derivatives by RANS simulation of planar motion mechanism test. Ocean. Eng. 108, 129–139.
Labanti, J., Islam, H., Guedes Soares, C., 2016. CFD assessment of Ropax hull resistance with various initial drafts and trim angles. In: Guedes Soares, C., Santos, T.A. (Eds.), Maritime Technology and Engineering 3. Taylor & Francis Group, London, UK, pp. 325–332.
Lee, S., Kim, B., 2015. A numerical study on manoeuvrability of wind turbine installation vessel using OpenFOAM. Int. J. Nav. Architect. Ocean. Eng. 7, 466–477.
Lewis, E., 1988. Principles of Naval Architecture. The Society of Naval Architects and Marine Engineers, Jersey City, NJ.
Miller, R.W., 2008. PMM calculation for the bare and appended DTMB 5415 using the RaNS solver CFDSHIP-Iowa. In: SIMMAN 2008 Proceedings.
Shen, Z., Wan, D., Carrica, P.M., 2015. Dynamic overset grids in OpenFOAM with application to KCS self-propulsion and maneuvering. Ocean. Eng. 108, 287–306.
SIMMAN 2008. [Online] Available at: http://www.simman2008.dk/[Accessed 2016].
Simonsen, C., Stern, F., 2005. RANS maneouvering simulation of Esso Osaka with rudder and a body-force propeller. J. Ship Res. 49 (2), 98–120.
Simonsen, C., Stern, F., 2008. RANS simulation of the flow around the KCS container ship in pure yaw. In: Proceedings of the SIMMAN 2008 Workshop, pp. F55–F62.
Simonsen, C.D., Otzen, J.F., Klimt, C., Larsen, N.L., 2012. Manoeuvring predictions in the early design phase using CFD generated PMM data. In: 29th Symposium on Naval Hydrodynamics, Gothenburg.
Sutulo, S., Guedes Soares, C., 2006. Development of a multifactor regression model of ship manoeuvring forces based on optimized captive-model tests. J. Ship Res. 50 (4), 311–333.
Wang, H.M., Xie, Y., Liu, J.M., Zou, Z.J., He, W., 2011. Experimental and numerical researches on the viscosity hydrodynamic in hydrodynamic forces acting on a KVLCC2 model in oblique motion. In: Proceedings of the International Conference in Remote Sensing, Environment and Transportation Engineering (RSETE), pp. 328–331.
Wilson, R., Carrica, P., Stern, F., 2006. Unsteady RANS method for ship motions with application to roll for a surface combatant. Comput. Fluids 35 (5), 501–524.
Yao, J., Jin, W., Song, Y., 2016. RANS simulation of the flow around a tanker in forced motion. Ocean. Eng. 127, 236–245.